A Pulsed Source-Sink Fluid Mixing Device

Baratunde A. Cola, David K. Schaffer, Timothy S. Fisher, and Mark A. Stremler

Abstract—**Efficient fluid mixing can be achieved in a high-aspect-ratio volume by periodically pulsing an arrangement of source-sink pairs. In order to conserve fluid and promote mixing, the fluid extracted through a sink is subsequently injected through a source. We present an implementation of this approach that consists of a disposable chip with embedded microchannels and external fluidic control. When both the mixing chamber geometry and the source-sink arrangement are fixed, mixing is controlled by choosing α, the fraction of the mixing chamber volume that is exchanged with each pulse. Experimental results in a rectangular chamber show that the value of α has a significant effect on mixing efficiency. This device shows promise for enhancing the performance of massively parallel sensing systems such as DNA microarrays. [1592]**

Index Terms—**Chaotic advection, Hele–Shaw flow, microelectromechanical systems (MEMS), microfluidics, mixing.**

I. Introduction

ACHIEVING efficient and uniform mixing of laminar flows in small-scale, high-aspect-ratio volumes is an important issue in the design of various micro- and meso-scale fluid systems. Consider, for example, DNA microarray analysis, a high-throughput, massively parallel screening technology that is helping redefine the approach to discovery in biomedical research [1]–[3]. This technique relies on the interaction of unknown DNA strands (the *targets*) suspended in a fluid solution with an array of known DNA strands (the *probes*) immobilized on a planar surface. Microarrays are being used successfully in a number of research applications [4], [5], but the standard implementation is unnecessarily slow and dominated by experimental noise; consistent results require tests to be run for as long as three days, with typical tests lasting 12–14 h [6], and as much as 94% of available data is thrown out as statistically unreliable [7]. These limitations arise largely from relying on molecular diffusion of the DNA to produce the necessary target-probe interactions. Several researchers have demonstrated that improved microarray analysis can be achieved by transporting the target molecules with an imposed flow [8]–[10], and one expects that significant improvement can be obtained when the fluid is mixed appropriately. This paper presents an experimental analysis of mixing in a high-aspect-ratio system that has been applied to DNA microarray analysis [10].

The difficulties encountered when trying to achieve rapid fluid mixing in small-scale systems are well known [11]. The small length scales restrict most practical devices to operate well within the range of laminar flow [12], which naturally tends to segregate regions of the fluid. Diffusion will, of course, cause mixing between these regions, but the diffusive time scale is too long to provide adequate levels of mixing in many applications. Furthermore, fabrication constraints limit the use of standard macroscale mixing enhancement techniques such as mechanical stirring. Specific focus has thus been given to developing devices that mix fluids effectively and are practical for implementation on the microscale. Progress has been made in both device design and the underlying theory (see, e.g., the recent theme issue on "Transport and mixing at the microscale" [13]), but this remains an active area of research.

One approach to achieving efficient and uniform mixing of laminar flow is to base the device design on the phenomenon of *chaotic advection* [14]–[16] in which passive particles advected by a periodic velocity field exhibit chaotic trajectories. These chaotic trajectories are associated with rapid (i.e., exponential) stretching and folding of the fluid, which have long been identified as crucial mechanisms for mixing enhancement [17]. This bulk deformation, typically viewed as stirring, acts to homogenize the fluid on a coarse scale while simultaneously increasing local concentration gradients and driving molecular diffusion.

A theoretical analysis [18] shows that potential flow in the unbounded plane exhibits chaotic advection when it is driven alternately by a source and a sink, with fluid extracted through the sink subsequently reinjected through the source. Based on this result, Liepmann proposed the "planar laminar mixer" [19], a MEMS device consisting of a rectangular mixing chamber with two sources and two sinks controlled by integrated bubble pumps and bubble valves. We have adapted this design to use off-chip pumps and valve actuators in a "plug-and-play" approach that avoids many of the complications and expenses incurred with a fully self-contained lab-on-a-chip device [20]. We focus here on a system geometry that is applicable to standard microarray analysis.

The design and fabrication of our device is presented in Section II, and the device operation is described in Section III. In Section IV we present an experimental evaluation of mixing in this system. Finally, in Section V, we summarize the findings of this work and discuss how these results compare with other mixing devices that target microarray analysis [8], [21], [22].

Manuscript received May 1, 2005; revised September 26, 2005. This work was supported by a grant from the National Institutes of Health and by Vanderbilt University. Subject Editor G. B. Hocker.

B. Cola and T. Fisher were with the Department of Mechanical Engineering, Vanderbilt University, Nashville, TN 37235 USA. They are now with the Department of Mechanical Engineering, Purdue University, West Lafayette, IN 47907 USA.

D. Schaffer was with the Department of Mechanical Engineering, Vanderbilt University, Nashville, TN 37235 USA. He is now with the Department of Physics and Astronomy, Vanderbilt University, Nashville, TN 37235 USA.

M. Stremler is with the Department of Mechanical Engineering, Vanderbilt University, Nashville, TN 37235 USA (e-mail: mark.stremler@vanderbilt.edu).

Digital Object Identifier 10.1109/JMEMS.2005.863786

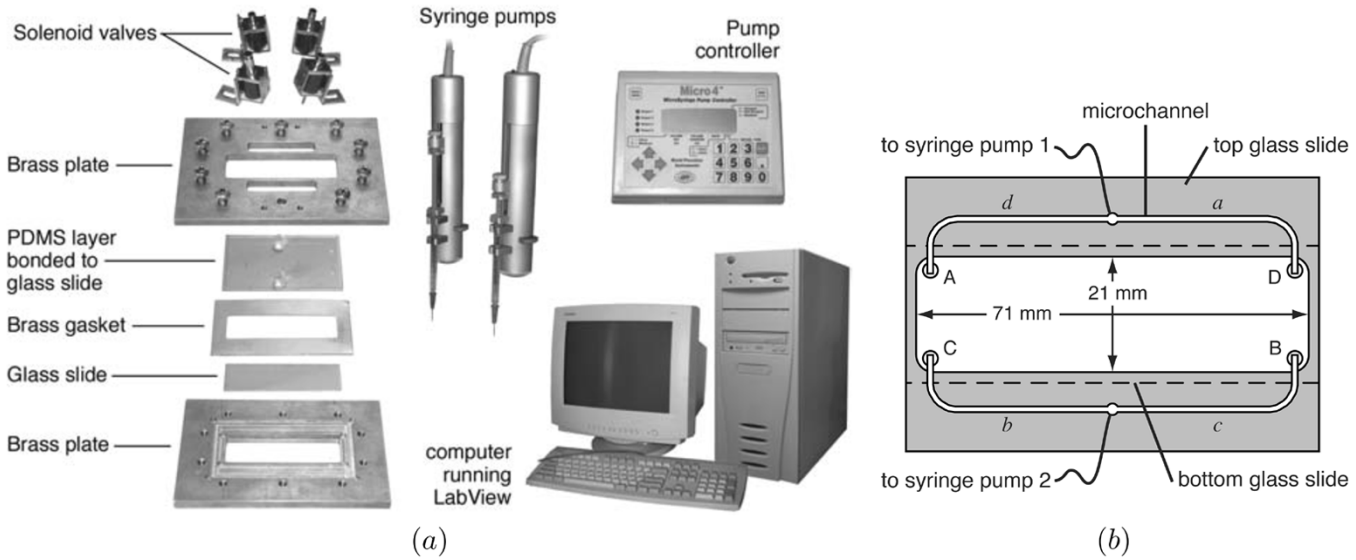

Fig. 1. Schematics of the components that comprise the experimental system. (a) Overview of the system, not to scale. (b) Top view of the mixing chamber and supporting microfluidics. Sources are at A and C, and sinks are at B and D. The four complementary microchannel branches are labeled a–d. The outline of the bottom glass slide is indicated by a dashed line. The area covered by the brass gasket is shown in gray. Source and sink diameters and microchannel widths are exaggerated for clarity.

II. Design and Fabrication

The pulsed source-sink mixing device, or *PSSMD*, that we investigate here consists of a high-aspect-ratio fluid volume, or *mixing chamber*, with four small access holes through which fluid is injected or extracted. Injecting fluid through a hole creates a *source* in the volume, and extracting fluid creates a *sink*. Flow is driven through the chamber by simultaneous operation of a source and a sink, which we refer to as a *source-sink pair*, and operation is periodically alternated between two different source-sink pairs. In order to efficiently mix a minimal fluid volume, fluid extracted through a sink is later reinjected through a source. Mixing is achieved in this system by combining piecewise constant operation of these two source-sink pairs with periodic relocation of fluid from a sink to a source.

A schematic of our device design and experimental setup is shown in Fig. 1. The mixing chamber is formed by clamping a brass gasket between two glass microscope slides. The bottom of the chamber is a 25 mm $\times$ 75 mm $\times$ 1 mm slide, and the top is a 50 mm $\times$ 75 mm $\times$ 1 mm glass slide. The gasket is stamped brass foil, which is available in various thicknesses; for the experiments presented in Section IV we used 50 μm-thick foil with a 21 mm $\times$ 71 mm hole, giving a mixing chamber volume $V_c \approx 75\,\mu$L. The brass gasket and the outer brass plates were fabricated in the Vanderbilt University Science Shop. The sources and sinks were formed by drilling four 1.25 mm-diameter holes in the top glass slide near each corner of the mixing chamber, as illustrated in Fig. 1(b). These holes lead to microchannels in a PDMS layer that are used to control the operation of the sources and sinks; these four holes hold a total fluid volume of approximately 5 μL. The microchannels are 250 μm wide and 25 μm deep, and they hold an additional combined fluid volume of approximately 1 μL.

The microfluidics layer was fabricated in polydimethylsiloxane (PDMS) elastomer using standard soft-lithograpy techniques [23], [24]. As illustrated in Fig. 1(b), the microchannels are U-shaped to allow an unobstructed view of the mixing chamber. Since the smallest feature size in the mask pattern is 250 μm, the mask can be easily fabricated by printing this pattern on standard transparency film with a high-resolution laser printer and then transferring the image to a chrome-on-glass mask (Nanofilm, Westlake Village, CA). The master mold was patterned by exposing a 25 μm-thick layer of SU-8 2025 (Micro-Chem, Newton, MA) through the chrome mask. The microchannel structure was then cast on this mold using Sylgard 184 (Dow Corning Corp., Midland, MI), a PDMS elastomer, creating 25-μm-deep microchannels. The PDMS was prepared per the manufacturer's recommendations. The base was mixed with curing agent in a 10:1 ratio by volume. The liquid PDMS was degassed at approximately 725 mm Hg for 20 min and then poured on the master and placed in an oven at 80 °C for a minimum of 2 hrs. The resulting PDMS layer is approximately 1 mm thick. The device was then cut from the bulk PDMS and a hole was bored through the PDMS at the center of each microchannel using a sharpened piece of 18-gauge stainless steel tubing. Templates for these holes are included in the mask design. Prior to plasma activation the microchannels were manually aligned with the holes in the 50 mm $\times$ 75 mm glass slide as illustrated in Fig. 1(b); manual alignment is sufficient due to the size of the holes. Finally, the PDMS layer was separated from the glass while maintaining alignment, activated in a Harrick PDC-32G RF air-plasma cleaner (Harrick Plasma, Ithaca, NY) for 20 s, and then allowed to contact and bond with the glass.

Fluid flow in the prototype PSSMD is driven by two Ultra-Micro Pump II systems (World Precision Instruments, Sarasota, FL), each outfitted with a 500 μL glass Hamilton syringe (Hamilton Co., Reno, NV). The pumps are individually controlled with a custom LabView Virtual Instrument (National Instruments Corporation, Austin, TX) on a desktop computer,

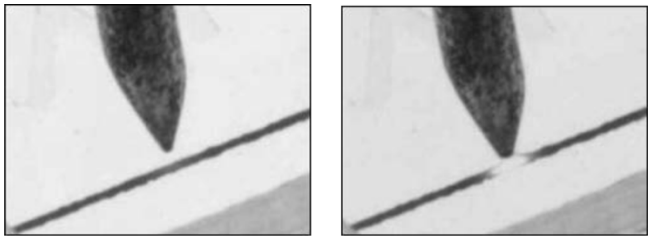

Fig. 2. Operation of a solenoid actuator pinch valve with a dye-filled microchannel. The valve is shown open (a) and closed (b) for the case of no imposed flow.

which is interfaced with the pumps through a World Precision Instruments Micro4 pump controller. Interconnects for joining the microchannels and the pumps were made by placing 13 mm sections of rigid 21-gauge stainless steel tubing in the holes bored through the PDMS at the center of each microchannel. Two 6 mm $\times$ 7.5 mm-diameter PDMS cylinders were then cast around these tubes to provide structural support. Each interconnect is joined to a syringe with flexible vinyl tubing having an inner diameter of 0.5 mm and an outer diameter of 1.5 mm.

In a DNA microarray application, all components that come in contact with the working fluid can only be used a single time. The disposable parts in our design thus include the bottom glass slide (or microarray), the gasket, the PDMS layer with the top glass slide, and the external tubing. Mixed fluid is not drawn into the syringes used with the pumps, so they can be reused, as can the solenoid actuators and the brass plates.

Alternate operation of source-sink pairs in the PSSMD requires reliable on/off valves. Consistent with our "plug-and-play" approach we have elected to use four externally mounted solenoid actuators (Bicron Electronics Company, Canaan, CT) to pinch closed the microchannels and shut off flow to each of the four ports when needed, as shown in Fig. 2. These solenoids are controlled with the NI Virtual Instrument via an NI interface card and a custom relay circuit. Power for the solenoids is provided by a 12-volt dc power supply (B&K Precision Corporation, Yorba Linda, CA). The tip of each solenoid core is sharpened to a small point in order to focus the actuator force on collapsing the channel and not on compressing the surrounding PDMS. When a solenoid actuator is released, the resilience of the PDMS elastomer and the fluid pressure combine to open the corresponding microchannel. This design can be easily modified to integrate the valve actuation by including an additional PDMS layer with pneumatic channels [25], although this approach requires multilayer fabrication of a disposable component.

III. Device Operation

This PSSMD is designed for periodic operation using the following two-step protocol. During step 1 of the protocol, a source is generated at A in Fig. 1(b) by pinching channel a shut with a solenoid valve and injecting fluid with flowrate Q using pump 1, and a sink is generated simultaneously at B by pinching channel b shut and extracting fluid with flowrate Q using pump 2. The device is operated steadily in this configuration for time T_p, which we refer to as the *pulse time*. During step 2 of the protocol, a source is generated at C by pinching channel c shut and injecting fluid with flowrate Q using pump 2, and a sink is generated at D by pinching channel d shut and extracting fluid with flowrate Q using pump 1. The device is operated steadily in this second configuration for time T_p, and operation is then switched back to step 1. Fluid extracted through B during step 1 is reinjected through C during step 2, and fluid extracted through D during step 2 is reinjected through A during step 1.

The parameters that can be varied in this basic design include the locations and connectivity of the sources and sinks, the rate at which fluid is delivered to the chamber, and the amount of fluid injected/extracted by a source-sink pair before switching to the alternate pair. In the present analysis we consider only the fixed source-sink configuration shown in Fig. 1(b) and we neglect any effects of changing the flowrate Q. Thus, device operation depends here only on $T = T_p + T_d$, the period of switching between different source-sink pairs, where T_d is a delay time that can occur between fluid pulses. During each pulse a source (or sink) will inject (or extract) a fluid pulse volume $V_p = QT_p$. It is convenient to work in terms of the relative pulse volume $\alpha = V_p/V_c$ and dimensionless time $\tau = Qt/V_c$. With this scaling, the dimensionless pulse time is $T_p{}^* = QT_p/V_c = \alpha$. That is, the relative pulse volume, α, can also be viewed as the time it takes to complete one pulse relative to the time it takes to inject (and extract) a fluid volume V_c.

The relevant Reynolds number (Re) for flow in the mixing chamber is $\mathrm{Re} = \epsilon\overline{V}/\nu$, where ϵ is the thickness of the chamber, $\overline{V}$ is the depth-averaged flow velocity, and ν is the kinematic viscosity of the fluid. The maximum Re in the chamber will occur at a source or a sink, which each have a diameter of approximately 25ϵ, giving $\mathrm{Re}_{\max} = \mathcal{O}(Q/25\pi\epsilon\nu)$. The velocity drops off quickly as the flow leaves the vicinity of a source, and through most of the mixing chamber $\overline{V} \approx Q/\epsilon h$, where $h = 21\,\mathrm{mm}$. For the experiments discussed in Section IV, water is used with a flowrate $Q = 3\ \mu\mathrm{L/s} = 0.18\ \mathrm{mL/min}$, so that it takes $V_c/Q = 25\ \mathrm{s}$ to inject the full chamber volume V_c. Under these operating conditions, $\mathrm{Re}_{\max} = \mathcal{O}(1)$ and the typical Reynolds number in the chamber is $\mathrm{Re}_{\mathrm{typ}} = \mathcal{O}(10^{-1})$. Note that in the microchannels $\mathrm{Re} = \mathcal{O}(10)$.

The characteristic diffusion time in this system is L^2/D, where L is a characteristic length and D is the molecular diffusivity. The length scale of interest is $L = \sqrt{A_c}$, where $A_c = V_c/\epsilon$ is the large projected area of the mixing chamber as viewed in Fig. 1(b). According to the above time scaling, the dimensionless diffusion time is thus $\delta = QA_c/DV_c = q/D$, where $q = Q/\epsilon$ is the average flowrate per unit depth. The ratio

$$\mathrm{Pe} = \frac{\delta}{\alpha} = \frac{\frac{L^2}{D}}{T_p} \tag{1}$$

is thus a Péclet number relating the characteristic diffusion time to the pulse time T_p, which is a characteristic advection time. The role of fluid motion in mixing increases with increasing Pe; we are concerned here with the case $\mathrm{Pe} \gg 1$, so that bulk diffusion is negligible. Note, however, that molecular diffusion plays an important role in Taylor dispersion, both in the mixing chamber [26] and in the external fluidic network [27].

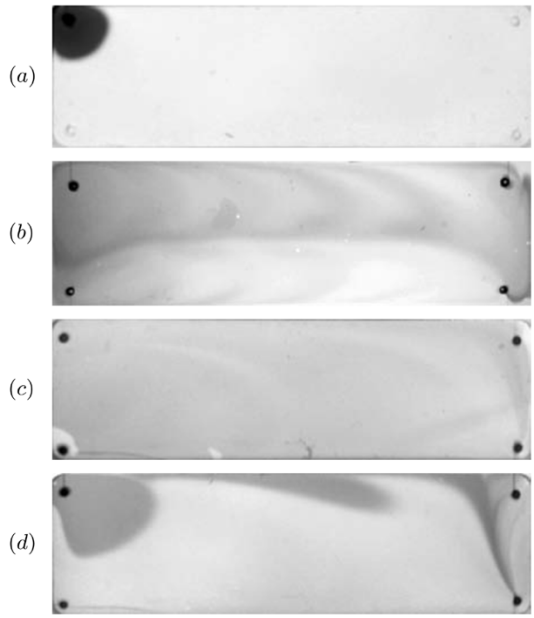

Fig. 3. Dye distribution in the mixing chamber. The contrast in the images has been enhanced in order to highlight variations in intensity. (a) A typical initial dye distribution. (b)–(d) Dye distribution after 19 pulses for (b) $\alpha \approx 10\%$ ($\tau_0 \approx 1.9$), (c) $\alpha \approx 17\%$ ($\tau_0 \approx 3.2$), and (d) $\alpha \approx 26\%$ ($\tau_0 \approx 4.9$). The apparent lack of dye in the lower left corner of (c) is an optical effect caused by an imperfection in the device that does not affect operation.

During the device operation, there is a delay time between successive pulses in which the pressure and velocity fields equilibrate, valve states switch, and the pumps reverse. If we represent the dimensionless delay time by β, the total (dimensionless) time required to complete n pulses is given by

$$\tau_\beta(n) = (\alpha + \beta)n. \tag{2}$$

In our prototype system with $Q = 3\,\mu\mathrm{L/s}$, a delay time less than approximately 10 s, or $\beta \lesssim 40\%$, led to an apparent build-up of pressure after several pulses that caused fluid to leak from the domain. Thus, our experiments were conducted with $\beta \geq 40\%$. In an ideal system the delay time is negligible; the corresponding ideal time, $\tau_0 = \alpha n$, gives a lower bound on the time it takes to complete n pulses for a given α. In the other extreme, $\beta \gg \alpha$, the time needed to complete n pulses is essentially identical for all values of α. Using the results in Section IV to consider the case of large β requires having $\delta \gg \beta$, so that diffusive mixing during the delay is negligible.

IV. Mixing Experiments

Mixing in this PSSMD is evaluated by monitoring the distribution of dye in the mixing chamber. The dye used in these experiments is erioglaucine (Sigma-Aldrich, Inc., St. Louis, MO), also known as Acid Blue 9, a high-molecular weight blue dye. The system was initially filled with water, and a small amount of water-dye mixture was injected at A as an initial condition [see Fig. 3(a)]. The time it takes to achieve a well-mixed state in this device depends, in part, on this initial condition for the dye. The initial dye volume was typically 5% of V_c, and the initial dye concentration was approximately 10% by volume for each experimental run. The small dye volume is difficult to mix rapidly throughout the entire domain, which allows us to clearly distinguish the mixing capabilities of this device at different pulse volumes. We observed the dye concentration to be small enough that viscosity and density mismatches between the water and the water-dye mixture, which can lead to a fingering instability in the concentration front (see, e.g., [28]), are negligible.

The dye was mixed in the chamber by operating the sources and sinks according to the protocol described in Section II. The source-sink pair A-B was pulsed first for each experimental run. The distribution of dye was recorded after each pulse with a Fuji FinePix S1 Pro digital camera (Fuji Photo Film Co., Ltd., Tokyo) which records 24 bit RGB images at a resolution of 3040×2016 pixels. The dye signal was isolated by converting these images to a CMYK color profile using Adobe Photoshop software (Adobe Systems, Inc., San Jose, CA) and analyzing only the cyan channel.

The value of α used in each experimental run was determined by measuring the displacement of a dye front in successive images. That is, we estimate V_p for a given experiment as $V_p = \epsilon A_p$, where A_p is the projected area of the domain that is traversed by a dye front during a single pulse, as determined from the digital images. Monitoring different dye fronts at different stages of an experiment gives an estimate of the error in α, which is due to both inaccuracy in determining the dye front location and variation in performance of the valves and pumps. We found this calibration of the system for each experimental run to be essential for accurately determining α.

Example dye distributions after 19 pulses are shown in Fig. 3 for $\alpha = 10\% \pm 2\%$, $17\% \pm 2\%$, and $26\% \pm 3\%$. The mixing produced with $\alpha \approx 17\%$ is noticeably better than that with $\alpha \approx 10\%$ or 26%. A single pulse is also completed more quickly for $\alpha \approx 17\%$ than for $\alpha \approx 26\%$; thus, based on this comparison with $n = 19$, using a pulse volume $\alpha \approx 17\%$ mixes faster than $\alpha \approx 26\%$ for all values of β. Determining which of $\alpha \approx 10\%$ or 17% mixes more efficiently, however, requires further consideration.

The quality of mixing can be quantified by the coefficient of variation in intensity for an image

$$\mathrm{COV} = \frac{\sigma}{I_{\mathrm{ave}}} \tag{3}$$

where I_{ave} is the average intensity in the image and σ is the standard deviation of the intensity. In order to account for variations in initial conditions between experimental runs, we quantify the mixing using a normalized coefficient of variation, or *mixing index*

$$\eta = \frac{\mathrm{COV}}{\mathrm{COV}_{\max}} \tag{4}$$

where $\mathrm{COV}_{\max}$ is the maximum coefficient of variation in intensity for a given experimental run. For these experiments we estimate that the error in η is within ± 0.05. The most poorly mixed condition in an experimental run is normalized to $\eta = 1$, and as the fluid is mixed η decreases. Ideally, perfect mixing is achieved when $\eta = 0$, but in practice there is some background variation that gives $\eta \neq 0$ as the well-mixed limit.

The influence of pulse volume on mixing in our PSSMD is shown in Fig. 4 for five different values of α. When the delay time is negligible (i.e., $\beta = 0$), Fig. 4(a) shows that, for the pulse

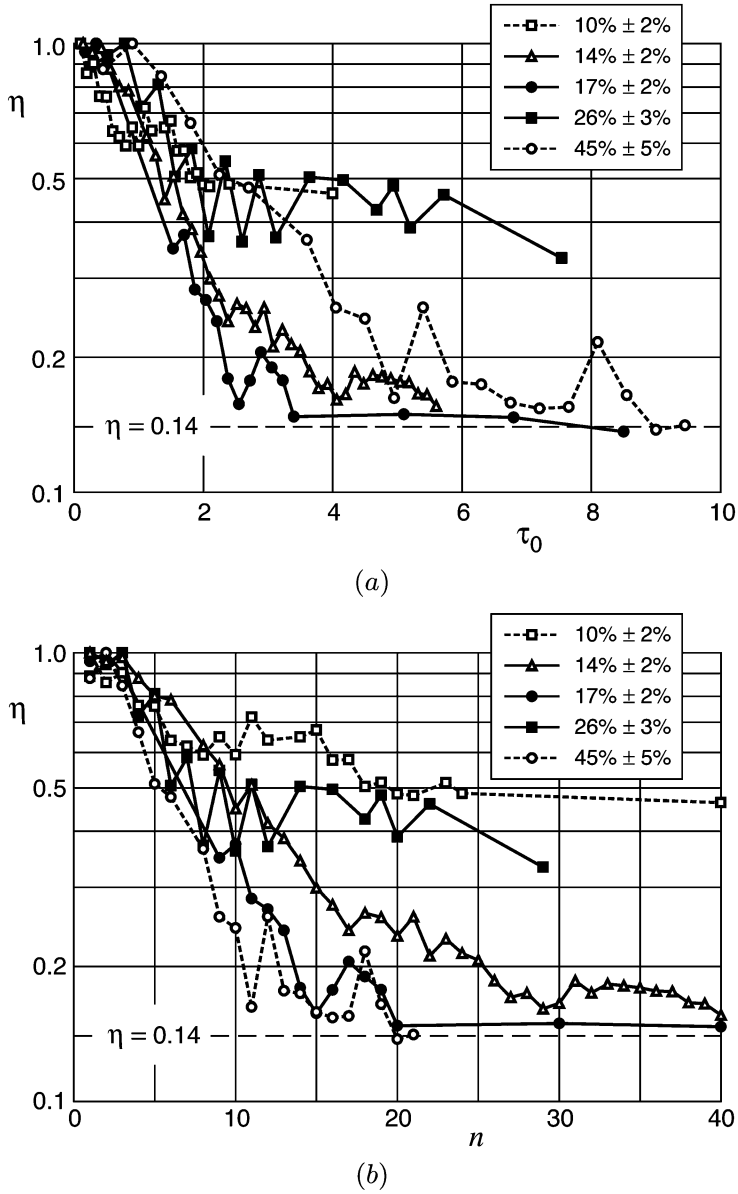

Fig. 4. Evolution of the mixing index for five choices of dimensionless pulse volume α. Curves are labeled according to the corresponding value of α. The data is shown (a) as a function of ideal time for the case when $\beta = 0$, and (b) as a function of pulse number. Note that these two panels are different representations of the same data.

volumes tested, optimal mixing is achieved when $\alpha \approx 17\%$. Rapid mixing is also achieved for $\alpha \approx 14\%$. If the delay time is dominant (i.e., $\beta \gg \alpha$), so that each period of operation takes roughly the same amount of time independent of α, Fig. 4(b) shows that both $\alpha \approx 17\%$ and 45% mix well. Taking $\alpha \approx 45\%$ appears to mix slightly faster than $\alpha \approx 17\%$ in this case, although the intensity data for each of these is essentially equivalent within the noise of the experiment.

As shown in Fig. 3, dye tends to accumulate in the holes in the top glass plate as fluid is pulsed through the domain. In calculating η we do not include these holes or the corners of an image that lie outside of the mixing chamber. Excluding the holes from the calculations results in η values that are slightly lower than if the accumulation did not occur.

We note that $\mathrm{COV}_{\max}$ does not occur for the initial condition in these experiments. The initial condition is produced by loading dye through microchannel d (see Fig. 1), and some dye remains in this channel after the loading step. During the first few pulses of the system, dye continues to be added to the domain. These pulses are also starting to mix the fluid, but the additional dye causes $\mathrm{COV}_{\max}$, and thus $\eta = 1$, to occur for a pulse in the range $1 \leq n \leq 3$.

In some cases, particularly for $\alpha \approx 26\%$, there is significant variation in η between successive pulses. This variation is due to dye being extracted from and reinjected into the domain, as shown in Fig. 5. Extracting a concentrated region of dye from the domain causes a decrease in $\mathrm{COV}_{\max}$ and an increase in I_{ave}, which gives a low value of η that does not accurately represent mixing in the system. The mixing performance must therefore be based on the overall trend in the mixing index.

Since we are trying to mix as quickly as possible, and larger pulses take more time to complete, an initial assumption might

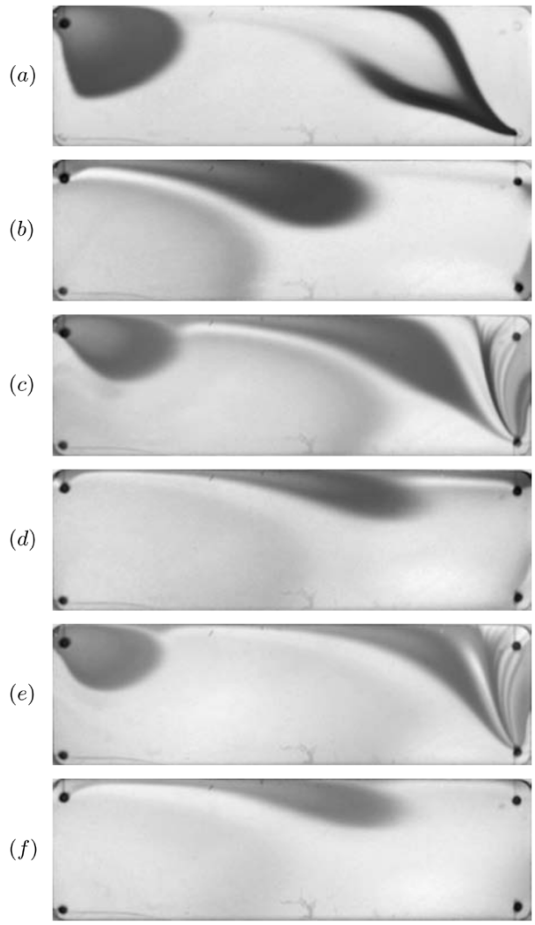

Fig. 5. Dye distribution in the mixing chamber with $\alpha \approx 26\%$ after pulse number (a) 3, (b) 4, (c) 5, (d) 6, (e) 7, and (f) 8. Image contrast has been enhanced to highlight intensity variations.

have been to keep α small. However, if $\alpha \approx 10\%$, most of the fluid injected through source A is essentially confined to the A–D side of the mixing chamber, which is apparent in Fig. 3(b). This segregation of the top and bottom halves of the domain is even more pronounced for smaller α. As α is increased from 10%, however, the system behavior changes rapidly, with very little long-time segregation of the domain occurring even for $\alpha \approx 14\%$.

A significant reduction in mixing efficacy occurs in this PSSMD as α is increased from 17% to 26%. Fig. 4 shows that the evolution of the mixing index for $\alpha \approx 26\%$ is similar to that for $\alpha \approx 10\%$. The image sequence in Fig. 5 reveals a repeating pattern in which dye injected at A is moved across the chamber by a sequence of 2 additional pulses and then extracted through sink D. At the end of the second pulse, some of the dye has been brought close to sink B, but very little, if any, dye is drawn into that sink for reinjection at source C. On the following pulse, most of the dye is extracted through sink D. This dye is then reinjected through source A, and the pattern begins again. Note that the dye structure that occurs for odd pulse number is still apparant for $n = 19$ shown in Fig. 3. The behavior of the system with $\alpha \approx 26\%$ is thus similar to that with $\alpha \approx 10\%$, in that the flow causes segregation between regions of the domain, which leads to poor mixing.

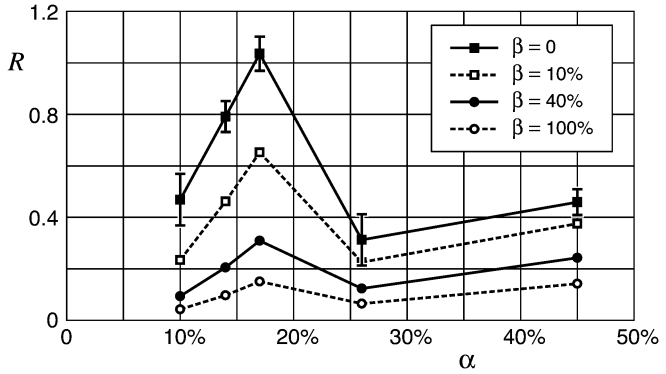

Fig. 6. Mixing rates determined by fitting (5) to the data in Fig. 4. Curves are labeled according to the value of the delay time β. Error estimates shown for $\beta = 0$ are based on the quality of the curve fit.

For a given experimental run, the decay in mixing index over time can be represented by [29], [30]

$$\eta = C\exp(-R\tau_\beta) + \eta_\star \tag{5}$$

where R is the *mixing rate*, $\eta_\star$ is the limiting value of η for the well-mixed flow, and C is a parameter that accounts for variations in the time at which $\eta = 1$. In the cases considered here that mix well, the mixing index appears to converge to $\eta \approx 0.14$, so we assume $\eta_\star = 0.14$ for every experimental run. Fitting (5) to the data in Fig. 4 gives the mixing rates shown in Fig. 6. Optimal mixing is obtained for maximum R. Thus, for $0 \leq \beta \lesssim 100\%$ and the pulse volumes tested, $\alpha \approx 17\%$ generates optimal mixing. For $\beta \gtrsim 100\%$ the highest mixing rate is achieved for $\alpha \approx 45\%$, although, as we noted previously, there is little difference between $\alpha \approx 17\%$ and $\alpha \approx 45\%$ for large β.

The mixing rate can be used to estimate the time needed for the system to become well mixed. Since we have assumed $\eta_\star = 0.14$ and the error in η is approximately ± 0.05, we refer to this system as being well mixed if $\eta \leq 0.19$. Since $C \approx 1$ for each of the experimental runs, (5) gives

$$\tau_\beta \approx \frac{3}{R} \tag{6}$$

as this "well-mixed time." For $\alpha \approx$14%, 17%, and 45%, the time given by (6) correlates well with the actual time required to achieve $\eta \leq 0.19$. For $\alpha \approx$10% and 26%, however, (6) appears to underestimate the time that would be required to mix well. For example, with $\alpha \approx 26\%$ and $\beta = 0$ the well-mixed time given by (5) is $\tau_0 \approx 9.7$, which is not consistent with the trend in the mixing index shown in Fig. 4. That is, the mixing achieved with $\alpha \approx 10$ or 26% is even worse than indicated by the mixing rate in Fig. 6.

We observed that the mixing for $\alpha > 45\%$ (not shown) is similar to, or worse than, the mixing obtained with $\alpha \approx 45\%$ after the same number of pulses. Since the operating time increases with increasing α, we have not given these large pulse volumes detailed consideration.

V. Conclusion

Experimental results for the high-aspect-ratio PSSMD design outlined in Section II, in which fluid is periodically extracted from one end of a rectangular domain and subsequently injected

at the other end, show that optimal mixing of the dye distribution shown in Fig. 3(a) is produced when each pulse exchanges approximately 17% of the chamber volume. If the system is operated with a significant delay between pulses, then taking $\alpha \approx 45\%$ also mixes well. Mixing is poor for very small α, despite the fact that multiple fluid pulses can be produced quickly. Mixing is also poor for $\alpha \approx 26\%$ because of a repeating pattern that occurs in the distribution of the dye. These experimental results are consistent with modeling results that predict the pulse volume for optimal mixing using an analysis of chaotic advection [31].

For $\alpha \approx 17\%$, with $Q = 3\,\mu\mathrm{L/s}$ and a delay time of 10s (corresponding to $\beta = 40\%$), fluid in this PSSMD is well mixed after approximately 250 s.[1] Much of this time is due to the long delay required between pulses in our prototype device. If, for example, the system were fabricated to accomodate a delay time of only 2 s (or $\beta = 8\%$), the fluid would be well mixed after approximately 110 s. Increasing the flowrate will also result in faster mixing. As long as the dimensional analysis presented in Section III is valid, the results in Figs. 4 and 6 can be used to determine the optimal pulse volume and the approximate time required to achieve a well-mixed flow. Note, however, that increasing the flowrate will increase pressure differences and shear rates in the flow, which might not be allowable in a given device despite the validity of the scaling arguments.

A few other devices presented in the literature are designed to enhance hybridization analysis on a standard microarray. Each of these generates a time-periodic flow pattern that can be viewed as flow due to an arrangment of sources and sinks. Differences in device geometry and initial dye distribution between each of these studies make it difficult to compare results, beyond stating that the mixing capabilities of each are similar. Adey *et al.* [8] consider a device with a flexible lid that uses two air-driven bladders to drive fluid back and forth across the microarray, which is similar to driving the flow with one source-sink pair. Liu *et al.* [21] use a piezoelectric disk to vibrate an array of bubbles immobilized on the top surface of the domain. Each bubble acts alternately as a source or sink, with switching occurring at very high frequency. The resulting streaming is a different flow phenonemon than in the other source-sink devices. Raynal *et al.* [22] drive fluid with periodic operation of two source-sink pairs in a device similar to that considered here. The primary difference between our PSSMD and the system in [22] is in the operation of the sources and sinks. In their device, any fluid extracted through a sink is later reinjected through that *same* hole; i.e., their mixing protocol does not include relocation of the fluid from sink to source. In contrast to our results, they find that mixing without relocation is more efficient when α is relatively large, with the implication that optimal operation occurs for $\alpha \approx 45\%$.

We note that pulsing fluid in and out of a mixing region has also been examined for microchannel flow [32]–[35]. The results in [34] show that when the system contains multiple "source-sink pairs" optimal mixing is achieved when different pairs are operated at different frequencies. This microchannel work suggests that the mixing performance of the PSSMD may be improved further by using more complex temporal operation of the source-sink pairs.

The pulsed source-sink device considered here is useful for mixing in small scale, high-aspect ratio volumes. The design is relatively easy to implement and is amenable to mass production of disposable devices. Application of this device to DNA hybridization analysis on microarrays has shown the potential for acheiving improved test results in an order of magnitude less time than with conventional static hybridization [10].

[1]As we noted in Section IV, the actual mixing time depends in part on the initial dye distribution.

REFERENCES

[1] J. L. DeRisi and V. R. Iyer, "Genomics and array technology," *Curr. Op. Oncology*, vol. 11, pp. 76–79, 1999.

[2] M. J. Heller, "DNA microarray technology: Devices, systems, and applications," *Ann. Rev. Biomed. Eng.*, vol. 4, pp. 129–153, 2002.

[3] J. H. Ng and L. L. Ilag, "Biochips beyond DNA: Technologies and applications," *Biotechnol. Ann. Rev.*, vol. 9, pp. 1–149, 2003.

[4] S. Mohr, G. D. Leikauf, G. Keith, and B. H. Rihn, "Microarrays as cancer keys: An array of possibilities," *J. Clin. Oncol.*, vol. 20, pp. 3165–3175, 2002.

[5] F. Bertucci, P. Viens, R. Tagett, C. Nguyen, R. Houlgatte, and D. Birnbaum, "DnNA arrays in clinical oncology: Promises and challenges," *Lab. Invest.*, vol. 83, pp. 305–316, 2003.

[6] M. Sartor, J. Schwanekamp, D. Halbleib, I. Mohamed, S. Karyala, M. Medvedovic, and C. R. Tomlinson, "Microarray results improve significantly as hybridization approaches equilibrium," *Biotechniques*, vol. 36, pp. 790–796, 2004.

[7] R. Iyer *et al.*, "The transcriptional program in the response of human fibroblasts to serum," *Science*, vol. 283, no. 5398, pp. 83–87, 1999.

[8] N. B. Adey *et al.*, "Gains in sensitivity with a device that mixes microarray hybridization solution in a 25-μm-thick chamber," *Anal. Chem.*, vol. 74, pp. 6413–6417, 2002.

[9] D. Erickson, X. Liu, U. Krull, and D. Li, "Electrokinetically controlled DNA hybridization microfluidic chip enabling rapid target analysis," *Anal. Chem.*, vol. 76, pp. 7269–7277, 2004.

[10] M. K. McQuain, K. Seale, J. Peek, T. Fisher, S. Levy, M. A. Stremler, and F. R. Haselton, "Chaotic mixer improves microarray hybridization," *Anal. Biochem.*, vol. 325, pp. 215–226, 2004.

[11] H. A. Stone and S. Kim, "Microfluidics: Basic issues, applications, and challenges," *AIChE J.*, vol. 47, no. 6, pp. 1250–1254, 2001.

[12] K. V. Sharp and R. J. Adrian, "Transition from laminar to turbulent flow in liquid filled microtubes," *Exp. Fluids*, vol. 36, pp. 741–747, 2004.

[13] J. M. Ottino and S. Wiggins, Eds., "A theme issue on transport and mixing at the microscale," *Phil. Trans. Roy. Soc. London A*, vol. 362, no. 1818, pp. 923–1129, 2004.

[14] M. A. Stremler, F. R. Haselton, and H. Aref, "Designing for chaos: Applications of chaotic advection at the microscale," *Phil. Trans. Roy. Soc. London A*, vol. 362, no. 1818, pp. 1019–1036, 2004.

[15] H. Aref, "The development of chaotic advection," *Phys. Fluids*, vol. 14, no. 4, pp. 1315–1325, 2002.

[16] J. M. Ottino, *The Kinematics of Mixing: Stretching, Chaos, and Transport*. Cambridge, U.K.: Cambridge University Press, 1989.

[17] O. Reynolds, "Study of fluid motion by means of colored bands," *Nature*, vol. 50, no. 1285, pp. 161–164, 1894.

[18] S. W. Jones and H. Aref, "Chaotic advection in pulsed source-sink systems," *Phys. Fluids*, vol. 31, no. 3, pp. 469–485, 1988.

[19] J. Evans, D. Liepmann, and A. P. Pisano, "Planar laminar mixer," in *Proc. IEEE Workshop MEMS*, 1997, pp. 96–101.

[20] C. R. Tamanaha, L. J. Whitman, and R. J. Colton, "Hybrid macro-micro fluidics system for a chip-based biosensor," *J. Micromech. Microeng.*, vol. 12, pp. N7–N17, 2002.

[21] R. H. Liu, J. Yang, M. Z. Pindera, M. Athavale, and P. Grodzinski, "Bubble-induced acoustic micromixing," *Lab on a Chip*, vol. 2, pp. 151–157, 2002.

[22] F. Raynal, F. Plaza, A. Beuf, P. Carrière, E. Souteyrand, J.-R. Martin, J.-P. Cloarec, and M. Cabrera, "Study of a chaotic mixing system for DNA chip hybridization chambers," *Phys. Fluids*, vol. 16, no. 9, pp. L63–L66, 2004.

[23] B.-H. Jo, L. M. Van Lerberghe, K. M. Motsegood, and D. J. Beebe, "Three-dimensional micro-channel fabrication in polydimethylsiloxane (PDMS) elastomer," *J. Microelectromech. Sys.*, vol. 9, pp. 76–81, 2000.

[24] J. R. Anderson *et al.*, "Fabrication of topologically complex three-dimensional microfluidic systems in PDMS by rapid prototyping," *Anal. Chem.*, vol. 72, pp. 3158–3164, 2000.
[25] M. A. Unger, H. P. Chou, T. Thorsen, A. Scherer, and S. R. Quake, "Monolithic microfabricated valves and pumps by multilayer soft lithography," *Science*, vol. 288, no. 5463, pp. 113–116, 2000.
[26] R. N. Horne and F. Rodriguez, "Dispersion in tracer flow in fractured geothermal systems," *Geophys. Res. Lett.*, vol. 10, pp. 289–292, 1983.
[27] G. I. Taylor, "Dispersion of soluble matter in solvent flowing slowly through a tube," *Proc. R. Soc. London A*, vol. 219, no. 1137, pp. 186–203, 1953.
[28] P. Petitjeans, C.-Y. Chen, E. Meiburg, and T. Maxworthy, "Miscible quarter five-spot displacements in a Hele-Shaw cell and the role of flow-induced dispersion," *Phys. Fluids*, vol. 11, pp. 1705–1716, 1999.
[29] C. D. Rielly, D. L. O. Smith, J. A. Lindley, K. Niranjan, and V. R. Phillips, "Mixing processes for agricultural and food materials: Part 4, assessment and monitoring of mixing systems," *J. Agric. Engng Res.*, vol. 59, pp. 1–18, 1994.
[30] G. A. Voth, T. C. Saint, G. Dobler, and J. P. Gollub, "Mixing rates and symmetry breaking in two-dimensional chaotic flow," *Phys. Fluids*, vol. 15, no. 9, pp. 2560–2566, 2003.
[31] M. A. Stremler and B. A. Cola, "A maximum entropy approach to optimal mixing in a pulsed source-sink flow," *Phys. Fluids*, vol. 18, Paper no. 011701, 2006.
[32] M. Volpert, I. Mezić, C. D. Meinhart, and M. Dahleh, "An actively controlled micromixer," in *Proc. ASME Mech. Eng. Internat. Congress & Expo., MEMS*, Nashville, TN, 1999, pp. 483–487.
[33] P. Tabeling, M. Chabert, A. Dodge, C. Jullien, and F. Okkels, "Chaotic mixing in cross-channel micromixers," *Phil. Trans. R. Soc. Lond. A*, vol. 362, pp. 987–1000, 2004.
[34] F. Bottausci, I. Mezić, C. D. Meinhart, and C. Cardonne, "Mixing in the shear superposition micromixer: Three-dimensional analysis," *Phil. Trans. R. Soc. Lond. A*, vol. 362, pp. 1001–1018, 2004.
[35] I. Glasgow, S. Lieber, and N. Aubry, "Parameters influencing pulsed flow mixing in microchannels," *Anal. Chem.*, vol. 76, pp. 4825–4832, 2004.

Baratunde A. Cola received the B.E. and M.S. degrees in mechanical engineering from Vanderbilt University, Nashville, TN, in 2002 and 2004, respectively, and he is currently working toward the Ph.D. degree in mechanical engineering at Purdue University, West Lafayette, IN.

His M.S. research included experimental and numerical investigations of mixing in microfluidic systems for enhancing DNA microarray analysis. His current research at the Purdue University Birck Nanotechnology Center is focused on thermal transport in carbon nanotube (CNT) arrays.

David K. Schaffer received the B.E. and M.S. degrees in mechanical engineering from Vanderbilt University in 2000 and 2003, respectively.

He is currently a Research/Development Engineer at the Vanderbilt Institute for Integrative Biosystems Research and Education (VIIBRE). His research interests include Microfluidic BioMEMS development for cellular instrumentation and analysis.

Timothy S. Fisher received the B.S. and Ph.D. degrees in mechanical engineering from Cornell University, Ithaca, NY, in 1991 and 1998, respectively.

He was a design engineer in Motorola's Automotive and Industrial Electronics Group (1991–1993) and an Assistant Professor of Mechanical Engineering at Vanderbilt University (1998–2002). He joined the Purdue School of Mechanical Engineering and Birck Nanotechnology Center in 2002. His research has included efforts in simulation and measurement of nanoscale heat transfer, coupled electro-thermal effects in semiconductor devices, nanoscale direct energy conversion, molecular electronics, microfluidic devices, hydrogen storage, and boundary- and finite-element computational methods. His current research efforts include theoretical, computational, and experimental studies focused toward integration of nanoscale materials with bulk materials for enhancement of electrical, thermal, and mass transport properties.

Mark A. Stremler received the B.S. degree in mechanical engineering and the B.S. degree in mathematics from Rose-Hulman Institute of Technology, Terre Haute, IN, in 1993, and the M.S. and Ph.D. degrees in theoretical and applied mechanics from the University of Illinois at Urbana-Champaign in 1995 and 1998, respectively.

He was a Research Associate at the Beckman Institute for Advanced Science and Technology, Universty of Illinois at Urbana-Champaign from 1998 to 2000. He is currently an Assistant Professor of Mechanical Engineering at Vanderbilt University. His research interests include theoretical, computational, and experimental investigations of laminar flows, particularly mixing in microfluidic systems, applications of chaos in fluid systems, and vortex dynamics.